

Magnetic excitations of diagonally coupled checkerboards

Tingting Yan(颜婷婷), Shangjian Jin(金尚健), Zijian Xiong(熊梓健), Jun Li(李军), and Dao-Xin Yao(姚道新)
Citation: Chin. Phys. B, 2021, 30 (**10**): 107505. DOI: 10.1088/1674-1056/ac1b94
Journal homepage: http://cpb.iphy.ac.cn; http://iopscience.iop.org/cpb

What follows is a list of articles you may be interested in

Ground-state phase diagram of the dimerizedspin-1/2 two-leg ladder

Cong Fu(傅聪), Hui Zhao(赵晖), Yu-Guang Chen(陈宇光), and Yong-Hong Yan(鄢永红)
Chin. Phys. B, 2021, 30 (**8**): 087501. DOI: 10.1088/1674-1056/abec31

Emergent O(4) symmetry at the phase transition from plaquette-singlet to antiferromagnetic order in quasi-two-dimensional quantum magnets

Guangyu Sun(孙光宇), Nvsen Ma(马女森), Bowen Zhao(赵博文), Anders W. Sandvik, and Zi Yang Meng(孟子杨)
Chin. Phys. B, 2021, 30 (**6**): 067505. DOI: 10.1088/1674-1056/abf3b8

Tunable deconfined quantum criticality and interplay of different valence-bond solid phases

Bowen Zhao(赵博文), Jun Takahashi, Anders W. Sandvik
Chin. Phys. B, 2020, 29 (**5**): 057506. DOI: 10.1088/1674-1056/ab889b

Magnetocaloric effect and critical behavior of the Mn-rich itinerant material Mn_3GaC with enhanced ferromagnetic interaction

Pengfei Liu(刘鹏飞), Jie Peng(彭杰), Mianqi Xue(薛面起), Bosen Wang(王铂森)
Chin. Phys. B, 2020, 29 (**4**): 047503. DOI: 10.1088/1674-1056/ab7da1

Exact solution of Heisenberg model with site-dependent exchange couplings and Dzyloshinsky-Moriya interaction

Yang Li-Jun, Cao Jun-Peng, Yang Wen-Li
Chin. Phys. B, 2015, 24 (**10**): 107502. DOI: 10.1088/1674-1056/24/10/107502

Magnetic excitations of diagonally coupled checkerboards*

Tingting Yan(颜婷婷)[1], Shangjian Jin(金尚健)[1], Zijian Xiong(熊梓健)[1,3], Jun Li(李军)[1,2,†], and Dao-Xin Yao(姚道新)[1,‡]

[1] State Key Laboratory of Optoelectronic Materials and Technologies, School of Physics, Sun Yat-Sen University, Guangzhou 510275, China
[2] Key Laboratory for Microstructural Material Physics of Hebei Province, School of Science, Yanshan University, Qinhuangdao 066004, China
[3] Department of Physics, Chongqing University, Chongqing 401331, China

(Received 12 July 2021; revised manuscript received 30 July 2021; accepted manuscript online 7 August 2021)

By using quantum Monte Carlo based stochastic analytic continuation (QMC-SAC) and spin wave theory, we study magnetic excitations of Heisenberg models with diagonally coupled checkerboard structures. We consider three kinds of checkerboard models (DC 2×2, DC 3×3, and CDC 3×3) consisting nearest-neighbor strong J_1 and weak J_2 antiferromagnetic interactions. When the coupling ratio $g=J_2/J_1$ approaches 1, all three diagonal checkerboards have the same long-range antiferromagnetic Néel order at $T=0$. When g decreases, the quantum fluctuation can drive DC 2×2 model to quantum paramagnetic state, while DC 3×3 and CDC 3×3 models still have the long-range Néel order. By calculating the magnetic excitations at different coupling ratios, we find that the low-energy part of magnetic excitations calculated by QMC-SAC can be well explained by the spin wave theory. However, the high-energy parts even deep in the long-range antiferromagnetic phase are beyond the spin wave description. Compared to the $g=1$ uniform square lattice, the high-energy excitations are more rich in our models. Our study may also draw the attention to the high-energy exctitaions beyond the spin wave theory.

Keywords: magnetic excitation, Heisenberg model, quantum Monte Carlo, spin wave

PACS: 75.30.Ds, 75.40.Gb, 76.50.+g, 02.70.Uu **DOI:** 10.1088/1674-1056/ac1b94

1. Introduction

The two-dimensional (2D) quantum magnetism is particularly important duo to its relevance to cuprate superconductors,[1–5] iron-based superconductors,[6–10] and many quantum magnetic materials.[11–14] It has become a cornerstone of the quantum phase transion, novel spin excitations, and other interesting phenomena. The spin-1/2 antiferromagnetic (AFM) Heisenberg model on the square lattice plays an important role in the 2D quantum magnetism.[15–20] It has been well studied that a long-range Néel order only exists at zero temperature due to Mermin–Wagner theorem.[21] Introducing some non-uniform or frustrated interactions may destroy the long-range Néel order and drive the system into other interesting phases such as valence bond solid (VBS),[22,23] spin liquid,[24,25] spin glass,[26,27] etc. Furthermore, higher-order topological insulators (HOTIs) can also be realized in the spatially non-uniform case.[28–30]

For the spin excitation of the square lattice Heisenberg model, the spin wave theory can qualitatively well describe the magnon dispersion. However, with the development of experimental measurement techniques, a large momentum-dependent continuum at $(\pi,0)$ and an anomalous damping of the spin waves at high energies were observed in the inelastic neutron scattering (INS) experiment of La_2CuO_4.[31,32] In addition, $Cu(DCOO)_2\cdot4D_2O$ (CFTD), a more ideal realization of the 2D AFM quantum Heisenberg model, has also showed similar exotic phenomena in its neutron scattering measurements where a non-spin-wave excitation continuum was revealed.[33–35] The high-energy anomaly has prompted speculations about fractionalized spin excitations. The continuum at $(\pi,0)$ is regarded as a signature of spatially extended pairs of fractional S = 1/2 quasiparticles.[35] Theoretically, a specific four-spin interaction Q (J–Q model) has been introduced to study the problem of spinon excitation,[36] and a frustrated Heisenberg model on square lattice was also used to elaborate the deconfinement of spinons.[37]

Exotic magnetic excitations beyond spin wave theory have been unveiled in more and more materials. The INS experiment of a dimerized AFM chain material, copper nitrate $Cu(NO_3)_2\cdot2.5D_2O$, has measured the one- and two-magnon excitation spectra.[38] Specifically, two-triplon scattering was observed quantitatively for the first time in the scattering on the ideal spin-ladder compound $La_4Sr_{10}Cu_{24}O_{41}$.[39] In addition, the one-dimensional Heisenberg–Ising antiferromagnet $SrCo_2V_2O_8$ in strong longitudinal magnetic fields was investigated to study the string states.[40] These discoveries have deepened our understanding of magnetic excitation and its nature laws, and inspired us to seek more details which may be ignored in many previous coarse studies.

The checkerboard models (or plaquette models) employed here are ideal platforms to simutaneously study the

*Project supported by the National Key R&D Program of China (Grant Nos. 2018YFA0306001 and 2017YFA0206203), the National Natural Science Foundation of China (Grant No. 11974432), GBABRF-2019A1515011337, and Leading Talent Program of Guangdong Special Projects.

†Corresponding author. E-mail: ljcj007@ysu.edu.cn
‡Corresponding author. E-mail: yaodaox@mail.sysu.edu.cn

© 2021 Chinese Physical Society and IOP Publishing Ltd

high-energy mode and the low-energy spin wave mode. For example, in one of our previous works, a 3×3 checkerboard model has been shown that the high-energy spin excitations can be triplon-like excitation determined by the stronger intra-sublattice interactions J_1, while the low-energy spin excitation is still spin wave mode determined by the weaker inter-sublattice interactions J_2.[41] In experiments, such checkerboard-like structure appears in $Bi_2Sr_2CaCu_2O_{8+\delta}$[42] and $Ca_{2-x}Na_xCuO_2Cl_2$.[43] Several types of noncollinear and modulated checkerboard models have also been constructed in theoretical studies.[44] The ground state and excitation spectra of orthogonal checkerboard models considering non-uniform interactions J_1 and J_2 have been studied by QMC methods recently,[41,45] and the magnetic excitation spectra exhibit novel features. The J_1–J_2 model is also extended to the one-dimensional case, where the system is equivalent to a quantum spin-1/2 chain with $J_{\text{eff}} = (4/9)J_2$ in the low-energy continuum, and the ground state is the Luttinger liquid state with two-spinon continuum, while the high-energy excitations correspond to the so-called doublons and quartons.[46]

However, the previous studies mainly focused on the orthogonal checkerboard models. If the spin blocks can be arranged along the diagonal direction, their ground states and excitation spectra would be different. Experimentally, non-orthogonally distributed 2×2 spin clusters have been found in iron-based material $KFe_{0.8}Ag_{1.2}Te_2$,[47] and the spin dynamics can be directly observed in INS experiments. On the other hand, it is feasible to construct the expected periodic checkerboard structure in the optical lattice through cold atom experiment.[48,49] The diagonal checkerboard systems have some unique properties. For example, since the spin clusters are more sparse, the quantum phase transition (QPT) point g_c would be much smaller theoretically, the local characteristics of the high-energy excitations of the internal magnetic structure are supposed to be more obvious. It is worth exploring the exotic magnetic excitation beyond the spin wave theory in these models.

Furthermore, with the development of numerical calculation methods as well as the increased power of computing resources, large-scale quantum Monte Carlo (QMC) simulations combined with stochastic analytic continuation (SAC) can provide results with unprecedented accuracy in the field of computational quantum many-body physics.[50–53] Compared to other numerical methods, such as exact diagonalization (ED),[54] density-matrix renormalization-group (DMRG),[55] matrix product state (MPS),[56] QMC-SAC method is not limited to small size systems and dimensions.[36,57–60] The calculated dynamic spin structure factor $S(\boldsymbol{q}, \omega)$ can be directly compared with INS experiments.[36,41]

In this paper, we study one 2×2 and two types of 3×3 diagonally coupled (DC) checkerboard models, as illustrated in Fig. 1. For convenience, we call them DC 2×2, DC 3×3, and CDC (compact diagonally coupled) 3×3 respectively. Each spin block connected by the thick red bonds J_1 is defined as a sublattice, and the sublattices are connected by the thin blue lines J_2. For DC 2×2, a quantum phase transition (QPT) between Néel phase and quantum paramagnetic phase occurs. The critical point belongs to O(3) universal class.[45] While for the two 3×3 systems, no QPT can be observed according to finite-size scaling analysis[45] because of an odd number of spins within a sublattice. Spin clusters are weakly coupled in DC 2×2 and DC 3×3, but closely coupled in CDC 3×3 where the sublattices share common spins. Nine spins in each 3×3 sublattice are supposed to renormalize to an effective 1/2 spin when the sublattices are isolated from each other. The distributions of J_1 and J_2 bonds will change the unit cell and magnetic Brillouin zone for these checkerboard models even when they are in the long-range Néel order. We use QMC-SAC to calculate the the dynamic spin structure factor $S(\boldsymbol{q}, \omega)$ and compare the results with the spin wave method. We expect to find exotic magnetic excitations beyond the spin wave theory.

The rest of the paper is organized as follows. In Section 2, we illustrate our model and the details of our methods. In Section 3, we introduce the QMC-SAC calculation and LSWT results for the three systems. The physical significance of spin excitation spectrum is analyzed in detail. Finally, in Section 4, we provide the conclusions.

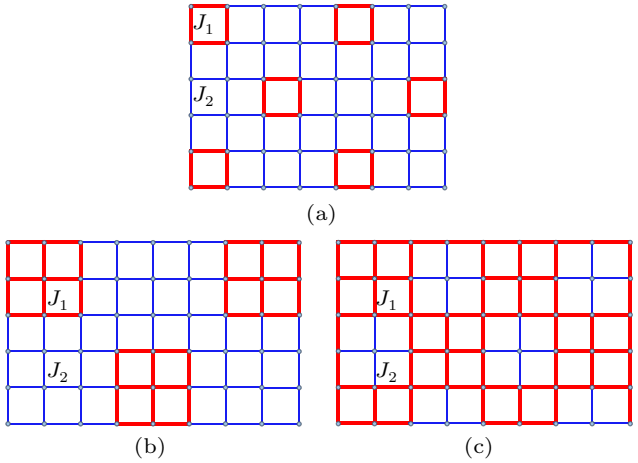


Fig. 1. Structures of the diagonally coupled checkerboard lattices. (a) DC 2×2, (b) DC 3×3, (c) CDC 3×3 models. The intra-sublattice interaction J_1 and the inter-sublattice interaction J_2 are represented by thick red and thin blue bonds, respectively.

2. Model and methods

2.1. Model

We consider the 2D spin-1/2 antiferromagnetic Heisenberg model on diagonally coupled checkerboard lattices with strong and weak antiferromagnetic exchange interactions J_1 and J_2, which correspond to the intra- and the inter-sublattice nearest-neighbor interactions, respectively, shown as the thick

red and thin blue bonds in Fig. 1. The Hamiltonian can be written as

$$\mathcal{H} = \sum_{\langle ij \rangle} J_{ij} \boldsymbol{S}_i \cdot \boldsymbol{S}_j, \tag{1}$$

where the symbol $\boldsymbol{S}_i$ represents the spin operator at the lattice site i. J_{ij} indicates the coupling between $\boldsymbol{S}_i$ and $\boldsymbol{S}_j$, which takes J_1 or J_2. The summation notation denotes taking sum of all pairs of nearest-neighbor lattice sites $\langle ij \rangle$.

In the following of this paper, we choose $J_1 = 1$ as the energy unit and use $g = J_2/J_1$ as a tuning parameter which takes from 0 to 1. The diagonally coupled checkerboard lattices will restore to a uniform Heisenberg model on square lattice at $g = 1$. While the interactions between sublattices disappear at $g = 0$, the spin sublattices are separated from the spins fully connected by the blue bonds.

2.2. Numerical methods

In order to obtain the spin excitation spectrum, the stochastic series expansion quantum Monte Carlo (SSE QMC) method is used to calculate the imaginary-time correlation function $G_{\boldsymbol{q}}(\tau)$ firstly,[50,61] which describes the dynamic spin–spin correlation of a given transferred momentum $\boldsymbol{q}$,

$$G_{\boldsymbol{q}}(\tau) = \langle \boldsymbol{S}^z_{-\boldsymbol{q}}(\tau) \boldsymbol{S}^z_{\boldsymbol{q}}(0) \rangle, \tag{2}$$

where $\boldsymbol{S}^z_{\boldsymbol{q}} = \frac{1}{\sqrt{N}} \sum_{i=1}^{N} \boldsymbol{S}^z_i \, \mathrm{e}^{-\mathrm{i} \boldsymbol{r}_i \cdot \boldsymbol{q}}$ is the Fourier transform of the spin operator, and $\boldsymbol{r}_i$ is the position vector. The relation between dynamic spin structure factor $S(\boldsymbol{q}, \omega)$ and imaginary-time correlation function $G_{\boldsymbol{q}}(\tau)$ is

$$G_{\boldsymbol{q}}(\tau) = \int_{-\infty}^{+\infty} S(\boldsymbol{q}, \omega) K(\tau, \omega) \mathrm{d}\omega, \tag{3}$$

where the kernel $K(\tau, \omega)$ is taken as $\frac{1}{\pi} \mathrm{e}^{-\tau\omega}$. At inverse temperature $\beta = 1/T$, the dynamic spin structure factor satisfies $S(\boldsymbol{q}, -\omega) = \mathrm{e}^{-\beta\omega} S(\boldsymbol{q}, \omega)$. By reducing the range of integration to $(0, \infty)$, we obtain

$$G_{\boldsymbol{q}}(\tau) = \frac{1}{\pi} \int_0^{+\infty} S(\boldsymbol{q}, \omega) \, \mathrm{e}^{-\tau\omega} \mathrm{d}\omega. \tag{4}$$

For a set of imaginary times τ_i, $i = 1, \ldots, N_\tau$, the SSE method applied here can offer us the stochastic approximation $\bar{G}_i \equiv \bar{G}(\tau_i)$ of the true correlation function $G_i \equiv G(\tau_i)$ with unbiasedness, as well as the correlated statistical errors of these data points. With the QMC data divided into N_b bins for $b = 1, 2, \cdots, N_b$, we have $\bar{G}_i = \sum_b G_i^b / N_b$, where G_i^b is the bin average. The covariance matrix is given by

$$C_{ij} = \frac{1}{N_b (N_b - 1)} \sum_{b=1}^{N_b} (G_i^b - \bar{G}_i)(G_j^b - \bar{G}_j). \tag{5}$$

Carrying out the stochastic analytic continuation (SAC) of Eq. (4) is the next step to gain the spectral function $S(\boldsymbol{q}, \omega)$.[36,57–59]

In our SAC method, the spectral function is typically parameterized as the sum of a large number of δ functions and their positions on a dense grid of frequencies are adjustable.[36,60] We sample an appropriate spectrum according to the following probability distribution:

$$P(S) \propto \exp\left(-\frac{\chi^2}{2\Theta}\right), \tag{6}$$

where S represents a sampled spectrum, Θ is called the sampling temperature, and χ^2 is the goodness of fit which denotes the closeness to the corresponding QMC computed function. The goodness of fit is written as

$$\chi^2 = \sum_{i=1}^{N_\tau} \sum_{j=1}^{N_\tau} \left(G_i - \bar{G}_i\right) \left(G_j - \bar{G}_j\right). \tag{7}$$

The χ^2 can verify the reliability of the results, and its minimum value is supposed to be found. As χ^2 varies with Θ which acts as a regularization parameter in Eq. (6), we adjust Θ until

$$\langle \chi^2 \rangle \approx \chi^2_{\min} + \sqrt{2\chi^2_{\min}}. \tag{8}$$

In this way, the best average spectrum $S(\boldsymbol{q}, \omega)$ is found and overfitting of imaginary-time correlation function is avoided.

The downside of the method is that $G_{\boldsymbol{q}}(\tau)$ obtained by QMC is always accompanied by a certain statistical error, and the information contained in the imaginary-time correlation is limited which leads to a ill-posed problem. Therefore, in the process of analytic continuation, we must adopt an appropriate modulation mechanism to eliminate those solutions with high noise.[60]

2.3. Linear spin wave theory

To compare with the results of numerical method, we apply a linear spin wave theory (LSWT)[62–64] to calculate the spectra. For the sake of simplicity, we use an antiferromagnetic ground state in the calculation of LSWT. LSWT applies the Holstein–Primakoff (HP) transformation to bosonize the Hamiltonian,

$$\begin{cases} S_i^+ \approx \sqrt{2S} a_i, \\ S_i^- \approx a_i^\dagger \sqrt{2S}, \\ S_i^z = S - a_i^\dagger a_i, \end{cases} \quad \begin{cases} S_j^+ \approx b_j^\dagger \sqrt{2S}, \\ S_j^- \approx \sqrt{2S} b_j, \\ S_j^z = b_j^\dagger b_j - S, \end{cases} \tag{9}$$

where $a_i, a_i^\dagger$ ($b_j, b_j^\dagger$) are creation and annihilation operators of the up (down) spins, respectively.

After taking a Fourier transform and a Bogoliubov transformation, we diagonalize the Hamiltonian and obtain the one-magnon dispersion. The dynamic structure factor is also calculated by LSWT

$$S^{\alpha\alpha}(\boldsymbol{q}, \omega) = \int_{-\infty}^{\infty} \frac{\mathrm{d}t}{2\pi} \left\langle S^\alpha_{\boldsymbol{q}}(t) S^\alpha_{-\boldsymbol{q}}(0) \right\rangle \mathrm{e}^{\mathrm{i}\omega t}. \tag{10}$$

We sum up three components $S^{\alpha\alpha}(\boldsymbol{q}, \omega)$ ($\alpha = x, y, z$) as our spectrum $S(\boldsymbol{q}, \omega)$.

3. Results and analyze

By using QMC-SAC method mentioned in Subsection 2.2, we calculate the dynamic structure factor $S(\boldsymbol{q}, \omega)$

along the path $(0,0) \to (0,\pi) \to (\pi,\pi) \to (0,0)$ due to the C_{4v} symmetry. In our numerical calculation, periodic boundary conditions are used in the $L \times L$ lattice, with $L = 48$. The inverse temperature is set as $\beta = L$.

3.1. The 2×2 diagonally coupled checkerboard model

The DC 2×2 structure contains four spins in each sublattice, see Fig. 1(a). The nearest sublattices are arranged in a cross distribution. As expected, $g = 1$ means a uniform AFM Heisenberg model which has a Néel ground state. As g decreases, the DC 2×2 model undergoes a quantum phase transition from long-range Néel order to a quantum paramagnetic state.[51,65–69] The quantum paramagnetic state is dominated by a linear superposition of the plaquette singlets, and the wave function for an isolated plaquette can be calculated exactly.[41] In addition, the quantum critical point is evaluated to be $g_c \approx 0.098(5)$ by QMC calculation. Here we mention that the g_c of DC 2×2 is much smaller than the one of the orthogonal 2×2 checkerboard lattice in our previous work, where $g_c = 0.548524$,[45] which reflects the sparsity of the 2×2 spin clusters. In the following, we only show the case of $g > g_c$ to sketch out the behavior of magnetic excitations beyond the spin wave theory even when the system is in the long-range Néel order.

The dynamic spin structure factors $S(\boldsymbol{q},\omega)$ of DC 2×2 model are presented in Figs. 2(a)–2(c). We take g as 0.1, 0.4, and 0.7 to show the evolution of $S(\boldsymbol{q},\omega)$. In the Néel order, we always observe two gapless excitation modes at different g based on the Goldstone theorem. For visibility, we set a upper limit of the intensity. The gapless excitation at (π,π) has a divergent spectral weight.[70] In contrary, the spectral weight at $(0,0)$ vanishes due to the conservation of total S^z. When $g \to g_c$, as shown in Fig. 2(a), there are two other gapless excitations at $(0,\pi)$ and $(\pi/2,\pi/2)$ which are due to the effect of Brillouin zone folding. As the reciprocal lattice vectors of the DC 2×2 system are $(-\pi/2,\pi/2)$ and $(\pi,0)$, thus the points at $(0,\pi)$ and $(\pi/2,\pi/2)$ host a similar excitation behavior with the ordering wave vector $\boldsymbol{Q} = (\pi,\pi)$. More interestingly, from QMC-SAC, we can observe a continuous high-energy branch above the low-energy one, and they are almost separated from each other. This can be related to the fractionalization of magnon, as the closer g is to g_c, the more unstable magnon is. For simplicity, we use a classical picture to understand the excitation in Fig. 2(a). Assume we flip one spin in the DC 2×2 system, the energy of one magnon would be $J_1 + J_2$ or $2J_2$. Thus the low-energy branch at $(0,\pi)$ point with $\omega \approx 2J_2$ results from the inter-sublattice interactions J_2. While the high-energy branch with $\omega \approx J_1 + J_2$ is due to the internal excitation within a sublattice.

To give a better understanding of the low-energy spin wave spectrum, we calculate the spin wave velocity for DC 2×2 model, which is written as

$$v_{sw} = \frac{g(3+g)}{2(1+g)} v_{AF}, \tag{11}$$

where $v_{AF} = 2\sqrt{2}J_1 S$ is the velocity of the square lattice antiferromagnet. The result of the spin wave velocity is shown in Fig. 6 and will be discussed later. We also present the excitation spectra of LSWT using SpinW program[71] to do the comparison. The results are given in Figs. 2(d)–2(f), where g is taken as 0.1, 0.4, and 0.7, respectively. The thin colored lines represent the dispersion relations and the color function reveals the spectral weight. Meanwhile, the partial dispersion relations are extracted and superimposed on the QMC-SAC results, shown as the white dash lines in Figs. 2(a)–2(c).

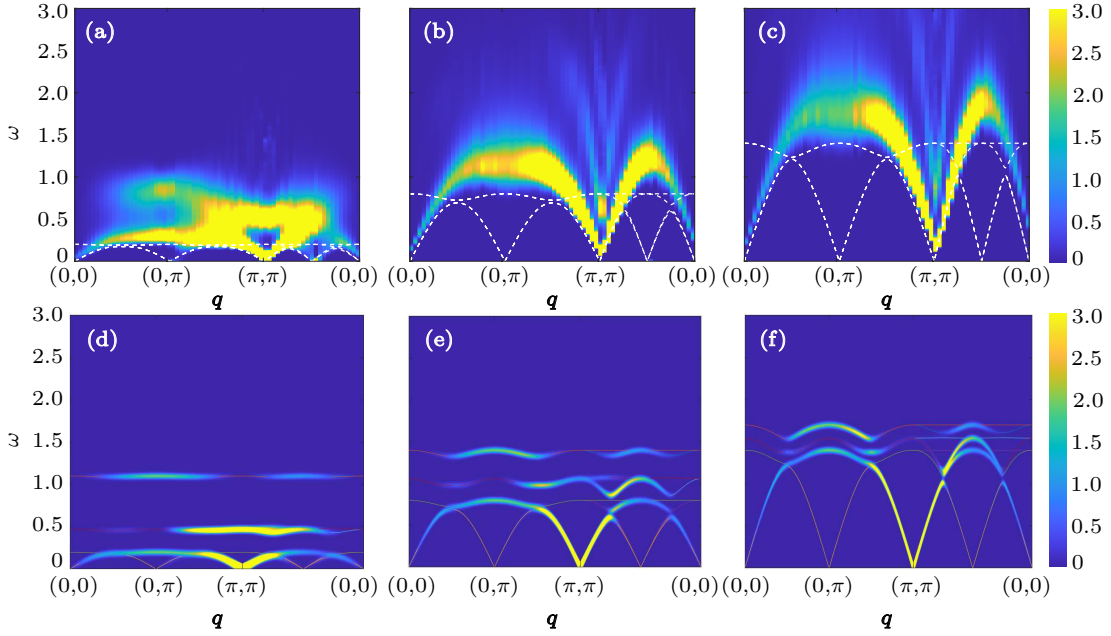


Fig. 2. Dynamic spin structure factor $S(\boldsymbol{q},\omega)$ obtained from QMC-SAC calculations for DC 2×2 model with g equal to (a) 0.1, (b) 0.4, and (c) 0.7, and (d)–(f) correspond to the LSWT results at the same g accordingly, while the white dash lines in (a)–(c) are the dispersion relations extracted from LSWT results.

From these results, we find that the LSWT gives consistent spin wave velocities and excitation behaviors with those of our QMC-SAC method at the gapless points, suggesting that LSWT can describe the system effectively at low energy. While for the high-energy part, LSWT provides flat dispersion relations. Such optical flat bands from LSWT already imply the localized properties of the high-energy excitations.

3.2. The 3×3 diagonally coupled checkerboard model

We then show the results of two types of 3×3 diagonally coupled checkerboard models. The first one is DC 3×3, see Fig. 1(b). The nearest-neighbor sublattices are diagonally arranged, and there are no sharing spins between them. Each sublattice contains nine spins. The odd number of spins within a sublattice makes it fail to form singlet pairs completely. According to our finite-size scaling analysis,[45] there is no quantum phase transition in this structure. The second one is the CDC 3×3, as shown in Fig. 1(c). The sublattice of this model also contains nine spins, but is more compacted than the DC 3×3 structure. And two sublattices are connected along the diagonal direction by sharing a spin. Especially, there are a few spins which are only surrounding by the weak interactions J_2. The QMC and LSWT results of these two models are illustrated in Figs. 3 and 4, where g is taken as 0.1, 0.4, and 0.7 from left to right.

When $g \to 1$, both of these two systems have obvious characteristics of the excitation spectrum of the Néel phase. The spectra are almost the same as those in DC 2×2 structure. The gapless excitations at $(0,0)$ and (π,π) are clearly observed. We also see a relatively large energy continuum of excitations at point $(0,\pi)$ in both structures. For DC 3×3 structure [Figs. 3(a)–3(c)], it can be clearly seen that the range of the spectrum reduces with the decrease of g. While for the CDC 3×3 structure in which sublattices share spins [Figs. 4(a)–4(c)], as g decreases, the lower boundary becomes lower while the upper boundary changes a little. Thus the spectrum becomes more broad. The difference between the two models comes from the stronger connection between sublattices in the CDC 3×3.

In DC 3×3 structure, LSWT also fits well with the QMC at low energy, however lots of dispersions in LSWT are invisible in the QMC spectra. Especially the broad continuum cannot be reproduced, which means that LSWT is not good enough to sketch a correct physical result at high energy even in the ordered phase here. Comparing the QMC spectra (Figs. 3(a)–3(c)) with LSWT ones (Figs. 3(d)–3(f)), as g increases, LSWT becomes closer to QMC results. In addition, the branch at $(0,\pi)$ point with $\omega \approx 2J_2$ also originates from the inter-sublattice interactions J_2. The gapless excitations at $(\pi/3,\pi)$ and $(2\pi/3,2\pi/3)$ can be understood by the reciprocal lattice vectors $(-\pi/3,\pi/3)$ and $(2\pi/3,0)$ with the ordering wave vector $\boldsymbol{Q} = (\pi,\pi)$.

In CDC 3×3 system, the intensity at $(0,\pi)$ point is much weaker than that in the DC 3×3 model. We attribute this to the relatively less inter-sublattice bonds here and the excitation is mainly determined by intra-sublattice interactions J_1. It can be observed in Figs. 4(a)–4(c) that the highest energy remains $\omega \approx 2J_1$, indicating a smaller quantum fluctuation even at $g = 0.1$ in this structure. It is more like a square lattice antiferromagnet. Similar to the structure of DC 2×2, their unit cells are in the same size, and the same gapless excitaions at $(0,\pi),(\pi,\pi)$, and $(\pi/2,\pi/2)$ are also due to the effect of the folded Brillouin zone. Again, the results of LSWT [Figs. 4(d)–4(f)] do not agree well with QMC-SAC results at high energy.

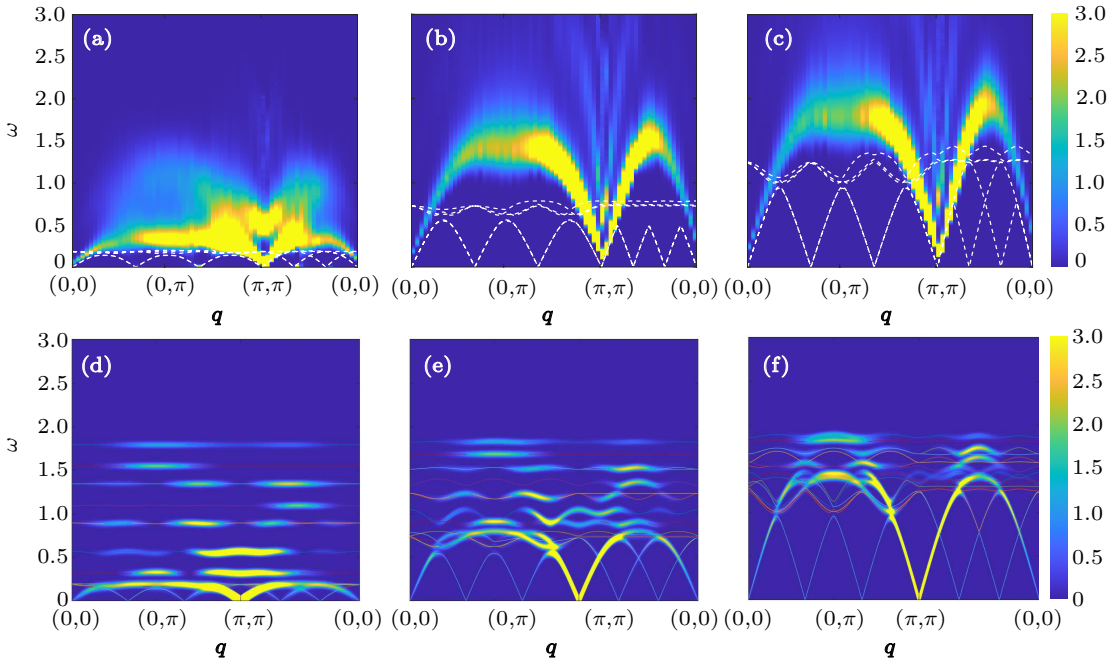


Fig. 3. Dynamic spin structure factors $S(\boldsymbol{q},\omega)$ obtained from QMC-SAC calculations for the DC 3×3 model with g equal to (a) 0.1, (b) 0.4, and (c) 0.7, and (d)–(f) correspond to the LSWT results at the same g accordingly, while the white dash lines in (a)–(c) are the dispersion relations extracted from LSWT results.

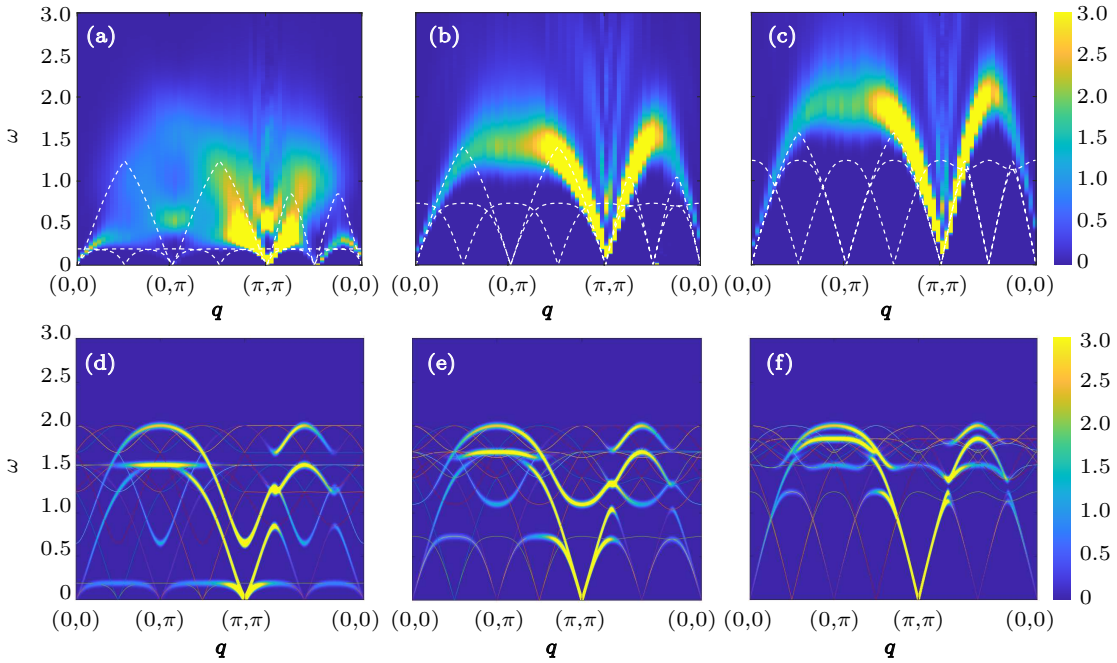


Fig. 4. Dynamic spin structure factors $S(\boldsymbol{q},\omega)$ obtained from QMC-SAC calculations for CDC 3×3 model with g equal to (a) 0.1, (b) 0.4, and (c) 0.7, and (d)–(f) correspond to the LSWT results at the same g accordingly, while the white dash lines in (a)–(c) are the dispersion relations extracted from LSWT results.

On account of that the liner spin wave theory is based on the assumption of a specific magnetic order, it can describe the Néel ground state well. Though the high-order corrections can be applied to improve the LSWT results,[72–75] it is still not enough to give full consistency with experimental and numerical results at high-energy spectra. New excitation pictures beyond spin wave theory, such as triplon,[41] are supposed to account for the high-energy anomaly. To capture the main features of the two 3×3 patterns, we build a "block spin" model with effective $1/2$ spins, as illustrated in Figs. 5(a) and 5(b). Each sublattice forms an effective $1/2$ up spin (red arrow) at the center while the surrounding spins connected by J_2 bonds form an effective $1/2$ down spin (blue arrow). Such block spin models form the square lattice Néel order with effective antiferromagnetic interactions $J_{\rm eff}$ ($J'_{\rm eff}$). For Fig. 5(a), the LSWT gives the one magnon dispersion $\hbar\omega(\boldsymbol{q}) = 4J_{\rm eff}S\sqrt{1-\frac{1}{4}\left[\cos(3q_x)+\cos(3q_y)\right]^2}$ with the spin wave velocity $v_{\rm AF}$ at gapless points. Figure 5(c) provides the corresponding dispersion (white dash line) with $J_{\rm eff}=0.1$ by SpinW program. For comparison, we extract the low-energy spectrum at $g=0.1$ of DC 3×3 from Fig. 3(a). We find that the low-energy branch can be fitted well by LSWT with the renormalized block model. Moreover, the effective block model gives the gapless excitations at $(0,2\pi/3)$, $(\pi/3,\pi)$, $(2\pi/3,2\pi/3)$, and $(\pi/3,\pi/3)$, which are consistent with QMC calculation. This behavior also exists in CDC 3×3 block model, see Fig. 5(d). However, as g increases, the spectral weight at these gapless points vanishes in both of the QMC and SpinW spectra. Thus, the models with smaller g are more close to the block models.

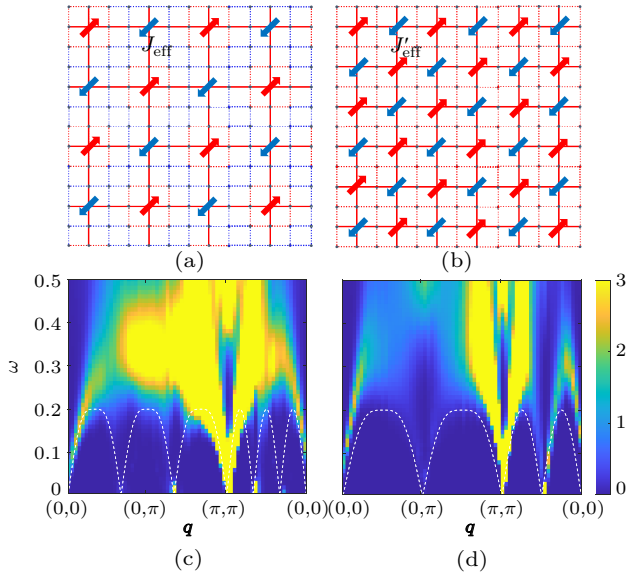


Fig. 5. Block spin models of the 3×3 systems: (a) DC 3×3, (b) CDC 3×3. The low-energy spectra for $g=0.1$ are extracted [(c) from Fig. 3 and (d) from Fig. 4]. Dispersion relations with effective interaction $J_{\rm eff}$ ($J'_{\rm eff}$) $=0.1$ from LSWT are showed by the white dashed lines.

In Fig. 6 we report the parameter-dependent spin wave velocity of the three models. The solid dots with error bars are obtained from QMC data by two steps. Firstly we use a Gaussian fitting of the QMC data to obtain the dispersion near the $\Gamma=(0,0)$ point. Then we do a linear fitting to the dispersion $\omega=\omega(\boldsymbol{q})$ and get the slope as the velocity. We also give the results from SpinW shown as the dashed lines. The solid line comes from Eq. (11) of DC 2×2, and it coincides exactly with the SpinW results. We find that the spin wave velocity of LSWT fits relatively well with QMC at large g. But for CDC 3×3 system, they separate obviously at small g. As g

increases, the spin wave velocity increases and then converges at $g = 1$ which can be understood by the fact that a larger J_2 enhances the excitation energies.

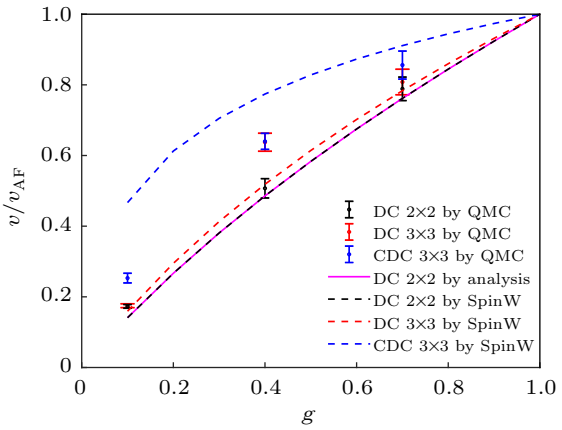


Fig. 6. The spin wave velocity of three systems with different g. Data points with error bars are given by QMC caculation. The solid line is the formula (11), while the dashed lines are the results of SpinW.

4. Conclusion

The spin excitation spectra of three diagonally coupled checkerboard AFM Heisenberg models have been studied by using QMC-SAC method and LSWT. We find that the DC 2×2 structure has a smaller quantum critical transition point g_c than the one of orthogonal 2×2 structure due to the sparsity of spin clusters. In addition to the low-energy spin wave excitation, we observe the high-energy excitations which deviate from the spin wave theory. For DC 3×3 and CDC 3×3 models, there is no quantum phase transition since their sublattices have odd number of spins. The two models always have the Néel order at zero temperature if $g \neq 0$. When g is small, the nine spins in each sublattice form an effective 1/2 spin, connected by the renormalized antiferromagnetic interactions. And the high-energy excitations from QMC start to deviate from the LSWT calcualtion, which is related to the high-energy internal excitations of sublattices such as triplon, etc. There are two energy scales in these models, which correspond to the low-energy spin wave excitation determined by J_2 and the high-energy internal excitations determined by J_1.

The diagonally coupled checkerboard lattice and magnetic excitation dynamics discussed in this paper may be realized in quantum magnetic materials and optical lattice experiments. The study of their high-energy magnetic excitations may also reveal novel physics beyond the spin wave theory.

Acknowledgement

We thank Han-Qing Wu, Jun-Qing Cheng, and Xiao-Xue Ran for careful reading and helpful discussions.

References

[1] Manousakis E 1991 *Rev. Mod. Phys.* **63** 1
[2] Barzykin V and Pines D 1995 *Phys. Rev. B* **52** 13585
[3] Andersen B M and Hedegård P 2005 *Phys. Rev. Lett.* **95** 037002
[4] Andersen B M, Hirschfeld P J, Kampf A P and Schmid M 2007 *Phys. Rev. Lett.* **99** 147002
[5] Lee-Hone N R, Dodge J S and Broun D M 2017 *Phys. Rev. B* **96** 024501
[6] Huang Q, Qiu Y, Bao W, Green M A, Lynn J W, Gasparovic Y C, Wu T, Wu G and Chen X H 2008 *Phys. Rev. Lett.* **101** 257003
[7] Zhao J, Huang Q, de la Cruz C, Li S, Lynn J W, Chen Y, Green M A, Chen G F, Li G, Li Z, Luo J L, Wang N L and Dai P 2008 *Nat. Mater.* **7** 953
[8] de la Cruz C, Huang Q, Lynn J W, Li J, II W R, Zarestky J L, Mook H A, Chen G F, Luo J L, Wang N L and Dai P 2008 *Nature* **453** 899
[9] Lumsden M D and Christianson A D 2010 *J. Phys.: Condens. Matter* **22** 203203
[10] Dai P 2015 *Rev. Mod. Phys.* **87** 855
[11] Wen J, Xu G, Gu G, Tranquada J M and Birgeneau R J 2011 *Rep. Prog. Phys.* **74** 124503
[12] Máca F, Mašek J, Stelmakhovych O, Martí X, Reichlová H, Uhlířová K, Beran P, Wadley P, Novák V and Jungwirth T 2012 *J. Magn. Magn. Mater.* **324** 1606
[13] Hu D, Lu X, Zhang W, Luo H, Li S, Wang P, Chen G, Han F, Banjara S R, Sapkota A, Kreyssig A, Goldman A I, Yamani Z, Niedermayer C, Skoulatos M, Georgii R, Keller T, Wang P, Yu W and Dai P 2015 *Phys. Rev. Lett.* **114** 157002
[14] Baltz V, Manchon A, Tsoi M, Moriyama T, Ono T and Tserkovnyak Y 2018 *Rev. Mod. Phys.* **90** 015005
[15] Manousakis E and Salvador R 1988 *Phys. Rev. Lett.* **60** 840
[16] Singh R R P and Huse D A 1989 *Phys. Rev. B* **40** 7247
[17] Greven M, Birgeneau R J, Endoh Y, Kastner M A, Keimer B, Matsuda M, Shirane G and Thurston T R 1994 *Phys. Rev. Lett.* **72** 1096
[18] Wessel S, Jagannathan A and Haas S 2003 *Phys. Rev. Lett.* **90** 177205
[19] Zhao B, Takahashi J and Sandvik A W 2020 *Chin. Phys. B* **29** 057506
[20] Sun G, Ma N, Zhao B, Sandvik A W and Meng Z Y 2021 *Chin. Phys. B* **30** 067505
[21] Liang S 1990 *Phys. Rev. B* **42** 6555
[22] Read N and Sachdev S 1989 *Phys. Rev. Lett.* **62** 1694
[23] Sandvik A W 2007 *Phys. Rev. B* **98** 227202
[24] Anderson P W 1987 *Science* **235** 1196
[25] Balents L 2010 *Nature* **464** 199
[26] 2004 *Phys. Rev. B* **69** 014424
[27] Campos I, Cotallo-Aban M, Martin-Mayor V, Perez-Gaviro S and Tarancon A 2006 *Phys. Rev. Lett.* **97** 217204
[28] Guo H M 2016 *Sci. China-Phys. Mech. Astron.* **59** 637401
[29] Guo J, Sun J, Zhu X, Li C A, Guo H and Feng S 2021 arXiv: 2010.05402
[30] Peng C, He R Q and Lu Z Y 2020 *Phys. Rev. B* **102** 045110
[31] Coldea R, Hayden S M, Aeppli G, Perring T G, Frost C D, Mason T E, Cheong S W and Fisk Z 2001 *Phys. Rev. Lett.* **86** 5377
[32] Headings N S, Hayden S M, Coldea R and Perring T G 2010 *Phys. Rev. Lett.* **105** 247001
[33] Rønnow H M, McMorrow D F, Coldea R, Harrison A, Youngson I D, Perring T G, Aeppli G, Syljuåsen O, Lefmann K and Rischel C 2001 *Phys. Rev. Lett.* **87** 037202
[34] Christensen N B, Rønnow H M, McMorrow D F, Harrison A, Perring T G, Enderle M, Coldea R, Regnault L P and Aeppli G 2007 *Proc. Natl. Acad. Sci. USA* **104** 15264
[35] Dalla Piazza B, Mourigal M, Christensen N B, Nilsen G J, Tregenna-Piggott P, Perring T G, Enderle M, McMorrow D F, Ivanov D A and Rønnow H M 2015 *Nat. Phys.* **11** 62
[36] Shao H, Qin Y Q, Capponi S, Chesi S, Meng Z Y and Sandvik A W 2017 *Phys. Rev. X* **7** 041072
[37] Yu S L, Wang W, Dong Z Y, Yao Z J and Li J X 2018 *Phys. Rev. B* **98** 134410
[38] Tennant D A, Broholm C, Reich D H, Nagler S E, Granroth G E, Barnes T, Damle K, Xu G, Chen Y and Sales B C 2003 *Phys. Rev. B* **67** 054414
[39] Notbohm S, Ribeiro P, Lake B, Tennant D A, Schmidt K P, Uhrig G S, Hess C, Klingeler R, Behr G, Büchner B, Reehuis M, Bewley R I, Frost C D, Manuel P and Eccleston R S 2007 *Phys. Rev. Lett.* **98** 027403
[40] Bera A K, Wu J, Yang W, Bewley R, Boehm M, Xu J, Bartkowiak M, Prokhnenko O, Klemke B, Islam A T M N, Law J M, Wang Z and Lake B 2020 *Nat. Phys.* **16** 625
[41] Xu Y, Xiong Z, Wu H Q and Yao D X 2019 *Phys. Rev. B* **99** 085112

[42] Hoffman J E, Hudson E W, Lang K M, Madhavan V, Eisaki H, Uchida S and Davis J C 2002 *Science* **295** 466
[43] Hanaguri T, Lupien C, Kohsaka Y, Lee D H, Azuma M, Takano M, Takagi H and Davis J C 2004 *Nature* **430** 1001
[44] Yao D X and Carlson E W 2008 *Phys. Rev. B* **77** 024503
[45] Ran X X, Ma N and Yao D X 2019 *Phys. Rev. B* **99** 174434
[46] Cheng J Q, Li J, Xiong Z, Wu H Q, Sandvik A W and Yao D X 2020 arxiV: 2011.02448
[47] Song Y, Yuan D, Lu X, Xu Z, Bourret-Courchesne E and Birgeneau R J 2019 *Phys. Rev. Lett.* **123** 247205
[48] Góral K, Santos L and Lewenstein M 2002 *Phys. Rev. Lett.* **88** 170406
[49] Ölschläger M, Wirth G, Kock T and Hemmerich A 2012 *Phys. Rev. Lett.* **108** 075302
[50] Sandvik A W 1997 *Phys. Rev. B* **56** 11678
[51] Wenzel S, Bogacz L and Janke W 2008 *Phys. Rev. Lett.* **101** 127202
[52] Jiang F J 2012 *Phys. Rev. B* **85** 014414
[53] Ma N, Sun G Y, You Y Z, Xu C, Vishwanath A, Sandvik A W and Meng Z Y 2018 *Phys. Rev. B* **98** 174421
[54] Lin H Q 1990 *Phys. Rev. B* **42** 6561
[55] Jeckelmann E 2002 *Phys. Rev. B* **66** 045114
[56] Verstraete F and Cirac J I 2010 *Phys. Rev. Lett.* **104** 190405
[57] Sandvik A W 1998 *Phys. Rev. B* **57** 10287
[58] Syljuåsen O F 2008 *Phys. Rev. B* **78** 174429
[59] Sandvik A W 2016 *Phys. Rev. E* **94** 063308
[60] Shu Y R, Dupont M, Yao D X, Capponi S and Sandvik A W 2018 *Phys. Rev. B* **97** 104424
[61] Sandvik A W 2010 *AIP Conf. Proc.* **1297** 135
[62] des Cloizeaux J and Pearson J J 1962 *Phys. Rev.* **128** 2131
[63] Melcher R L 1973 *Phys. Rev. Lett.* **30** 125
[64] Locher P 1990 *Phys. Rev. B* **41** 2537
[65] Wang L, Beach K S D and Sandvik A W 2006 *Phys. Rev. B* **73** 014431
[66] Syljuåsen O F 2006 *Phys. Rev. B* **73** 245105
[67] Yao D X, Gustafsson J, Carlson E W and Sandvik A W 2010 *Phys. Rev. B* **82** 172409
[68] Fritz L, Doretto R L, Wessel S, Wenzel S, Burdin S and Vojta M 2011 *Phys. Rev. B* **83** 174416
[69] Yasuda S and Todo S 2013 *Phys. Rev. E* **88** 061301
[70] Wallace D J and Zia R K P 1975 *Phys. Rev. B* **12** 5340
[71] Toth S and Lake B 2015 *J. Phys.: Condens. Matter* **27** 166002
[72] Canali C M and Wallin M 1993 *Phys. Rev. B* **48** 3264
[73] Lorenzana J, Seibold G and Coldea R 2005 *Phys. Rev. B* **72** 224511
[74] Igarashi J I and Nagao T 2005 *Phys. Rev. B* **72**014403
[75] Syromyatnikov A V 2010 *J. Phys.: Condens. Matter* **22** 216003